Mechanical Engineering Advances 2025, 3(4), 3338.
doi: https://doi.org/10.59400/mea3338

Article

A data-driven approach for predicting stress intensity factors of a single-edge cracked plate with a random polygon-shaped void

Mehrad Zargar Ershadi[1], Saeid Nickabadi[2,*], Majid Askari Sayar[2], Alireza Alidoust[3], Reza Ansari[1]

[1] Faculty of Mechanical Engineering, University of Guilan, Rasht P.O. Box 3756, Iran
[2] Faculty of Mechanical Engineering, University of Imam Khomeini Marine Sciences, Nowshahr 4651783311, Iran
[3] Department of Mechanical Engineering, Isfahan University of Technology, Isfahan 8415683111, Iran
*** Corresponding author:** Saeid Nickabadi, s.nikabadi@ikhnsu.ac.ir

CITATION

Ershadi MZ, Nickabadi S, Sayar MA, et al. A data-driven approach for predicting stress intensity factors of a single-edge cracked plate with a random polygon-shaped void. Mechanical Engineering Advances. 2025; 3(4): 3338. https://doi.org/10.59400/mea3338

ARTICLE INFO

Received: 4 June 2025
Revised: 9 November 2025
Accepted: 12 November 2025
Available online: 3 December 2025

Abstract: This study represents a data-driven framework for predicting mode I (K_I) and mode II (K_{II}) Stress Intensity Factors (SIFs) in single-edge cracked plates with central polygon-shaped voids. Finite element simulations were conducted in Abaqus software to generate a dataset by varying key parameters, including the polygon's number of vertices, angle, average radius, and crack length. Two machine learning models were employed to analyze the dataset created by the finite element method: Group Method of Data Handling (GMDH) networks and an Artificial Neural Network (ANN). The GMDH networks were optimized using the least squares method and the Root Mean Squared Error (RMSE) criteria, while the ANN, designed as a feedforward fully connected network, was trained with the backpropagation algorithm and the gradient descent optimization technique using TensorFlow and Keras libraries. The ANN demonstrated exceptional accuracy, with a R^2 value exceeding 0.99 for K_I predictions and 0.98 for K_{II}, significantly outperforming GMDH models, particularly in capturing the nonlinear behavior of K_{II}.

Keywords: machine learning algorithms; stress intensity factor; computational fracture mechanics; data-driven approach; polygon-shaped voids

1. Introduction

The study of fracture mechanics is critical in understanding the failure mechanisms of solid structures subjected to varying loading conditions, with significant utilization in industries such as aerospace science, automotive, and shipbuilding [1]. Structural failure due to cracking can have catastrophic consequences, emphasizing the need for systematic methodologies to evaluate and mitigate fracture risks. Historically, one of the earliest attempts to study stress concentrations due to the existence of cracks is attributed to research conducted by Inglis [2], where a rectangular plate with an elliptic central hole was investigated. Afterward, Griffith [3] laid the foundation of classical fracture mechanics, also known as Linear Elastic Fracture Mechanics (LEFM), by introducing a criterion for crack growth in brittle materials based on energy. The field of fracture mechanics gained prominence after World War II, as the widespread adoption of welding in shipbuilding resulted in numerous brittle fractures in welded ship components [4]. These failures led to the identification and development of concepts such as the Stress Intensity Factor (SIF), which describes the stress field near crack tips and serves as a primary criterion in LEFM [5]. LEFM is applicable when the non-linear

deformation is restricted to an insignificant region around the crack tip. If the plastic area surrounding the crack tip is not negligible, Elastic-Plastic Fracture Mechanics (EPFM) must be considered. Two elastic-plastic fracture parameters are defined: the Crack Tip Opening Displacement (CTOD) and the J-integral. The J-integral parameter, as introduced by Rice [6], defines a path-independent contour integral employed in analyzing the cracked bodies and generalizes the definition of G (energy release rate) in nonlinear elastic materials. The values of stress intensity factors can also be determined by calculating the J-integral parameter in the vicinity of the crack tip. By providing a quantitative framework for analyzing crack propagation, LEFM has become an essential tool in engineering design, helping prevent brittle fractures in structural and mechanical components under elastic loading conditions. The SIF links external loading, material properties, and crack geometry, allowing for accurate predictions of fracture behavior, making it a fundamental parameter in fracture mechanics' research [7–10]. The stress intensity factor, denoted as K, plays a pivotal role in determining the local stress distribution near the crack tip and predicting crack growth under various loading conditions. Its calculation is critical for assessing the structural integrity of components and ensuring their safe operation. Analytical methods for evaluating SIFs have provided valuable insights but are limited to simplified geometries and boundary conditions [11]. Experimental techniques, while direct, are resource-intensive and often unsuitable for complex geometries or variable parameters [12]. Numerical methods, particularly Finite Element Analysis (FEA), have emerged as powerful tools for computing SIFs in intricate configurations, offering flexibility in modeling realistic geometries, complex loadings, and material heterogeneity [13]. Although the present study employs two-dimensional finite element analysis in Abaqus/Standard, together with quarter-point crack-tip elements and contour-integral (J-integral) techniques to evaluate mode I and mode II stress intensity factors, it is important to note that several other robust numerical approaches have also been successfully developed for fracture and structural analysis. Among them, the Differential Quadrature Method (DQM) has been widely used as a high-accuracy, mesh-efficient technique for solving governing differential equations in plate and fracture problems, providing rapid convergence and reduced computational cost compared to conventional discretization schemes [14]. More recently, the Bézier multi-step method has been introduced as an advanced numerical framework for the analysis of thin-walled and structural systems, demonstrating strong stability characteristics and high precision in capturing complex mechanical responses [15]. These methods highlight that, alongside FEM, alternative numerical formulations can serve as powerful tools for fracture mechanics and structural integrity assessments. Nevertheless, FEM remains particularly attractive for cracked bodies with complex geometries due to its flexibility, maturity, and seamless integration with data-driven modeling frameworks, which motivates its selection in the present work.

The integration of Machine Learning (ML) algorithms and, in particular, Deep Learning (DL) techniques into fracture mechanics has gained growing interest as a means to address the computational limitations of traditional numerical methods [16,17]. While FEA-based approaches are robust, their application to systems with extensive

parameter spaces or high levels of geometric complexity can be computationally prohibitive. Data-driven techniques have shown remarkable potential in reducing computational costs while maintaining high accuracy. By using large datasets generated from simulations [18,19] or experiments [20–22], ML models can predict SIF values and the brittle fracture behavior of structures efficiently, eliminating the need for repetitive numerical simulations. This is particularly valuable for real-time applications, such as structural health monitoring and adaptive design processes, where rapid predictions are critical. Furthermore, ML methods allow for the exploration of high-dimensional parameter spaces, uncovering complex relationships between input variables and fracture behavior. Recent advancements in data-driven fracture mechanics have shown that surrogate models can significantly enhance the efficiency and scope of fracture analysis, making them invaluable tools for both research and practical applications. Kaloop et al. [23] explored the application of various soft computing models for predicting SIFs in offshore pipelines. The models included Functional Network (FN), Emotional Neural Network (ENN), Relevance Vector Machine (RVM), and Minimax Probability Machine Regression (MPMR). Comparative analysis revealed that RVM and MPMR outperformed FN and ENN in training and testing stages, with MPMR achieving the highest accuracy (1.31% prediction error). Zhang and co-workers [24] introduced a data-driven model for predicting mixed-mode SIFs in composites using artificial neural networks. The model combined datasets from the interaction integral and extended finite element method (XFEM), incorporating dimensionality reduction techniques like Principal Component Analysis (PCA). Hyperparameters were optimized using Bayesian optimization and K-fold cross-validation to enhance model generalization. Additionally, an active learning framework addressed data scarcity, demonstrating the effectiveness of data-driven models in reducing computational costs and solving high-dimensional nonlinear problems. In addition, the interaction between multiple cracks in infinite plates under mixed loading conditions was scrutinized [25]. They used the J-integral and FEA to assess intensification, protective, or neutral effects of secondary cracks on main cracks. An artificial neural network was trained on these results, providing accurate predictions for crack interactions and reducing computational efforts.

This study addresses the critical need for an efficient framework to investigate fracture behavior in plates with polygonal voids, which is highly relevant for structural design applications. While considerable advancements have been made in fracture mechanics and stress intensity factor modeling, existing methodologies often face challenges in accurately predicting SIFs without incurring substantial computational costs. There is a lack of reliable approaches that integrate computational techniques with data-driven models to predict stress intensity factors and analyze the intensification or protective effects of arbitrary void geometries on mode I (opening) and mode II (in-plane shear) fractures. To address this, over 30,000 Finite Element Method (FEM) simulations on steel plates were conducted, varying crack lengths and polygonal void characteristics, including number of vertices, average radius, and angular orientation. These FEM results were then used to train ANN and Group Method of Data Handling (GMDH) networks, offering a highly accurate and computationally efficient surrogate framework capable of predicting SIFs for arbitrary crack lengths and void

configurations. Additionally, this approach highlights the efficiency benefits of surrogate modeling, and future studies could explore active learning strategies to selectively generate training samples, potentially achieving similar predictive accuracy with fewer FEM runs while maintaining reliability.

2. Theory and simulation

2.1. The theory of linear elastic fracture mechanics

Fracture mechanics postulates the existence of a pre-initiated crack and does not study the crack formation itself, but rather focuses on its propagation. Griffith established the foundation of linear elastic fracture mechanics by proposing an energy-based criterion for crack growth in brittle materials. His theory assumes that cracks propagate when the total energy of a stressed body decreases, without accounting for stress concentration at the crack tip or the local processes ahead of the crack. Considering the energy balance for a body with a central crack of length $2a$, Griffith obtained a closed-form expression for the critical fracture stress (σ_f) as [3],

$$\begin{aligned} \sigma_f &= \left(\frac{2E\gamma_s}{\pi a}\right)^{\frac{1}{2}} \qquad for\ plane\ stress \\ \sigma_f &= \left(\frac{2E\gamma_s}{\pi a(1-\nu^2)}\right)^{\frac{1}{2}} \quad for\ plane\ strain \end{aligned} \tag{1}$$

where E is the elasticity modulus, ν denotes the Poisson's ratio, and γ_s represents the surface energy density for the specific material.

Williams [26] introduced an analytical approach to examine the stress field in the vicinity of the crack tip under generalized in-plane loading conditions. Considering appropriate symmetry condition (both the geometry and loading) in modes I and II of fracture (depicted in **Figure 1**), and assuming that the higher order terms are insignificant, the crack tip stress field may be expressed as,

$$\begin{aligned} \sigma_{rr} &= \frac{K_I}{\sqrt{2\pi r}}\left[\frac{5}{4}\cos\left(\frac{\theta}{2}\right) - \frac{1}{4}\cos\left(\frac{3\theta}{2}\right)\right] \\ \sigma_{\theta\theta} &= \frac{K_I}{\sqrt{2\pi r}}\left[\frac{3}{4}\cos\left(\frac{\theta}{2}\right) + \frac{1}{4}\cos\left(\frac{3\theta}{2}\right)\right] \\ \sigma_{r\theta} &= \frac{K_I}{\sqrt{2\pi r}}\left[\frac{1}{4}\sin\left(\frac{\theta}{2}\right) + \frac{1}{4}\sin\left(\frac{3\theta}{2}\right)\right] \end{aligned} \tag{2}$$

for mode I fracture, and also for mode II as follows,

$$\begin{aligned} \sigma_{rr} &= \frac{K_{II}}{\sqrt{2\pi r}}\left[-\frac{5}{4}\sin\left(\frac{\theta}{2}\right) + \frac{3}{4}\sin\left(\frac{3\theta}{2}\right)\right] \\ \sigma_{\theta\theta} &= \frac{K_{II}}{\sqrt{2\pi r}}\left[-\frac{3}{4}\sin\left(\frac{\theta}{2}\right) - \frac{3}{4}\sin\left(\frac{3\theta}{2}\right)\right] \\ \sigma_{r\theta} &= \frac{K_{II}}{\sqrt{2\pi r}}\left[\frac{1}{4}\cos\left(\frac{\theta}{2}\right) + \frac{3}{4}\cos\left(\frac{3\theta}{2}\right)\right] \end{aligned} \tag{3}$$

It is seen that for both loading modes, the $1/\sqrt{r}$ singularity is produced in the LEFM analysis, but the constants K and the θ-dependant expressions inside the

brackets ($f_{ij}(\theta)$) depend on the loading condition and the geometry. Williams was the first to identify the universal $1/\sqrt{r}$ singularity in elastic crack problems as a key factor in LEFM. In the 1950s, Irwin [27] advanced LEFM significantly by introducing the concept of the stress intensity factor (constant K in Equations (2) and (3)), a parameter that governs the crack-tip stress field and quantifies material toughness. Leveraging Williams' series solutions for stress and displacement fields surrounding crack tips in infinite plates, Irwin characterized the intensity of stress close to the crack tip in elastic bodies under external loads. This development made SIF one of the essential tools for predicting crack propagation and recognizing fracture characteristics in elastic materials.

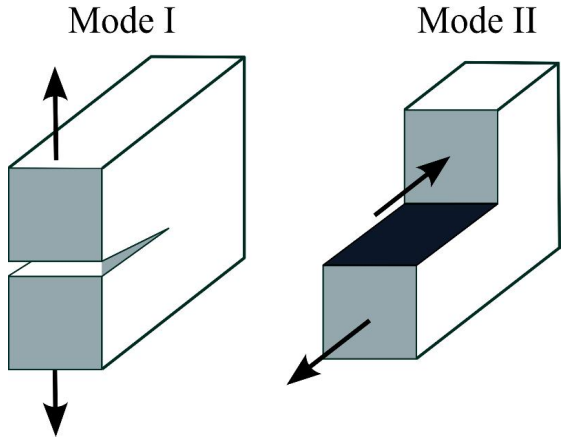

Figure 1. Schematic representation of mode I and II fracture.

Regarding simple cases, analytical solutions for K exist, but for more complex problems, they are estimated using experiments or numerical methods. For a few standard fracture test specimens, e.g., single-edge notched tension (SENT), single-edge notched bend (SENB), center-cracked tension (CCT), double-edge notched tension (DENT), and compact tension (CT), the closed-form expression for the mode I of fracture is given as [28],

$$K_I = \frac{P}{B\sqrt{W}} f\left(\frac{a}{W}\right) \tag{4}$$

where P, W, and a are the applied pressure, width, and crack length, specific to each test specimen. In addition, B represents the thickness of the specimen. The function $f(a/W)$ for each test configuration is also presented [28]. LEFM is primarily applicable when nonlinear deformation is confined to an inconsiderable region surrounding the crack tip, ensuring the validity of the linear elastic assumptions. Considering a cracked body, fracture toughness is defined as the critical energy release rate that the crack needs for extension. For a material undergoing brittle fracture, this parameter is characterized by the critical SIFs for the corresponding fracture modes: opening (mode I), in-plane shear (mode II), out-of-plane shear or tearing (mode III); in which are denoted by K_{Ic}, K_{IIc}, and K_{IIIc}, sequentially. It is worth noting that the experimental approach to calculate the plane-strain fracture toughness of metallic materials for mode I (K_{Ic}) employing various fatigue-cracked specimens is also detailed in ASTM-E399 [29].

For a plate with an inclined center crack positioned at an angle β relative to the horizontal line, assuming that the remote stress field is applied vertically, a combination of two or more loading modes are present for the crack, which is called the mixed-mode loading condition. In this case, the stress intensity factors are given as,

$$\begin{aligned} K_I &= \sigma\sqrt{\pi a}\cos^2\beta \\ K_{II} &= \sigma\sqrt{\pi a}\sin\beta\cos\beta \end{aligned} \tag{5}$$

In the present work, a two-dimensional plate under mode I loading condition is investigated. Additionally, a polygon-shaped void is considered in the middle of the place, with various angles and shapes, which may affect the loading condition and cause a mixed-mode SIF analysis. As a result, in this work, both K_I and K_{II} are scrutinized due to the existence of the central hole, knowing that the prominent fracture mechanism is the mode I fracture.

Another important parameter in fracture mechanics is the J contour integral. This parameter serves as a more general criterion than K, being used for elastic-plastic fracture estimation while remaining applicable and valid for LEFM as well. Rice [6] defined this path-independent contour integral and indicated that its value equals the energy release rate in nonlinear elastic materials. J as a line integral is expressed as,

$$J = \int_{\Gamma} \left(W dy - \mathbf{T} \cdot \frac{\partial \mathbf{u}}{\partial x} ds \right) \tag{6}$$

in which $W(\varepsilon_{mn}) = \int_0^{\varepsilon_{mn}} \sigma_{ij} d(\varepsilon_{ij})$ is the strain energy density. $\mathbf{T}$ is the traction vector acting on a point on bounding surface Γ, $\mathbf{u}$ represent the displacement vector, σ_{ij} are the components of the Cauchy stress tensor $\boldsymbol{\sigma}$. Values within this integral are obtained through FEM solutions effectively.

2.2. Polygon generator

To simulate an arbitrary void at the plate's center, a polygon generator function was developed using Python scripting method in Abaqus, based on methodologies presented [30, 31]. The algorithm initiates with a circular shape and selects points along its boundary. To introduce irregularities, angular deviations—referred to as "irregularity" and controlled by the parameter β_1 (ranging from 0 to 1)—are employed, resulting in vertices that are unevenly distributed. Furthermore, the randomness is amplified by altering the radial space of these points from the circle's center. This variation, termed "spikiness," is governed by the parameter β_2, which also ranges from 0 to 1. The entire process is mathematically formulated as [31],

$$\begin{aligned} \theta_i &= \theta_{i-1} + \frac{1}{k}\Delta\theta_i \\ \Delta\theta_i &= U\left(\frac{2\pi}{n} - \beta_1, \frac{2\pi}{n} + \beta_1\right) \\ r_i &= \text{clip}\left(N\left(d^*/2, \beta_2\right), 0, d^*/2\right) \end{aligned} \tag{7}$$

here, n denotes the number of vertices, $k = \sum(\Delta\theta_i/\pi)$, where θ_i represents the angle and r_i is the radius connecting the center of the circle to the i-th point. The random

angular spacing between consecutive points, denoted by $\Delta\theta_i$, is governed by a uniform distribution with upper and lower bounds of $\frac{2\pi}{n} - \beta_1$ and $\frac{2\pi}{n} + \beta_1$, sequentially. These perturbations introduce variability to the angular positions, enhancing the irregularity of the polygon. Also, a Gaussian distribution is employed for r_i, where the mean value corresponds to the diameter d^*, and the variance is controlled by β_2. Regular polygons can be generated by assigning a value of zero to both the irregularity and spikiness parameters. In this study, the irregularity and spikiness parameters are both allocated a fixed value of 0.01, effectively introducing a subtle noise-like effect to the generated polygon and correspondingly, the resulting dataset. **Figure 2** presents examples of generated polygons, illustrating variations in the number of vertices, angles, and average radii.

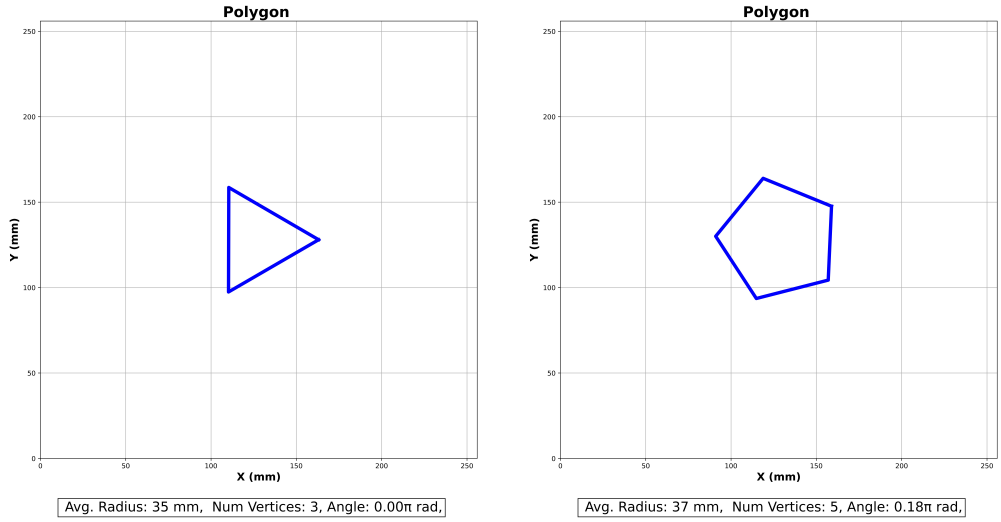

Figure 2. Generated polygons with varying number of vertices, angle, and average radius.

2.3. Dataset generation using finite elements modeling

As the initial step, finite element simulations are carried out utilizing the Abaqus/Standard FE software to construct a dataset of finite plates containing polygonal voids under uniaxial loading. CPS4R elements, characterized as 4-node bilinear plane stress quadrilateral elements with reduced integration and hourglass control, are employed in the analysis. The simulations assume a plane stress condition and disregard the influence of body forces.

Prior to dataset generation, in order to validate the present body of work, the existence of the central void was first omitted. A rectangular edge-cracked plate with its length, width, far field tensile stress, and crack length equal to 2, 1, 1, and 0.4 units, sequentially, is considered as a benchmark problem [28,32,33]. As reported by Tada et al. [28], the stress intensity factor of mode I fracture for this problem is 2.358, which is exactly obtained from the FEM simulation. Additionally, a second validation is done for non-dimensional stress intensity factors of cracks emerging from a central circular hole in a plate under tension in **Table 1** considering various crack lengths [34]. It is seen that the present model is well-validated. A mesh sensitivity analysis is also conducted. First, by making the entire model's seed size three times finer and hence increasing the approximate number of elements from 9786 to 67,611 (591%), it is seen

that the stress intensity factor values of the model only differ by a negligible amount of 0.03%. Secondly, by reducing the approximate seed size around the crack tip from 1 to 0.5 and employing finer meshes, it is observed that the stress intensity factors remain unchanged, indicating convergence and reaching a plateau. Finally, the seed size was selected as 3 over the plate's domain and 1 around the crack tip, which ensures reliable outputs.

Table 1. Comparison of normalized SIFs ($F = K/\sigma\sqrt{\pi a}$) considering $R/W = 0.5$ with those of Yan [34].

a/R	*F* (Yan) [34]	*F* (present work)	Error (%)
1.05	0.9630	0.9553	0.7996
1.1	1.2301	1.2238	0.5122
1.4	1.8247	1.8100	0.8056
1.7	2.4775	2.4656	0.4803

Finite element models of a plate featuring a central void are developed using an Abaqus script written with Python. This approach facilitates the automation of tasks, the variation of parameters, and the extraction of simulation data, thereby eliminating the need for repetitive manual operations [31]. A two-dimensional isotropic edge-cracked linear elastic plate under a tensile stress of $\sigma_0 = 100$ MPa is considered for this study, as illustrated in **Figure 3a**. In this study, the term 'arbitrary polygonal voids' refers to a broad class of irregular polygonal geometries generated within physically meaningful and engineering-relevant bounds. The parameter space was defined by varying the crack length, the average void radius, the number of polygon vertices, and the polygon orientation. These ranges were selected to span a wide spectrum of crack-void interaction scenarios commonly encountered in marine and mechanical structures, from sharp-cornered cavities to nearly circular irregular voids, and from short to relatively long edge cracks. Although bounded, this space generates highly diverse geometries and stress fields, allowing systematic investigation of fracture behavior while avoiding unrealistic or nonphysical configurations. The material properties include a Young's modulus of 207,000 MPa and a Poisson's ratio of 0.3. The plate incorporated a crack of length a, where this parameter varies between 50 to 70 mm. Multiple simulations were carried out to produce a diverse dataset encompassing various configurations of polygonal shapes. For each simulation, the solver initially defines the plate geometry and assigns material properties, namely the Young's modulus and Poisson's ratio. The script subsequently identifies the crack tip and generates a circle around it to facilitate improved meshing in the critical region. Additionally, a line is drawn extending from the crack tip, further enhancing the mesh quality and ensuring accurate representation of the stress field near the crack tip (**Figure 3b**). A random polygonal void is introduced at the center of the plate, with the number of vertices ranging from 3 to 10, an average radius between 30 and 40 mm, and an angle determined based on the number of vertices. Notably, the angle range varies for each number of vertices due to the axisymmetric characteristics of the problem. Within the interaction module, the crack is designated as a seam, and a contour integral crack is defined to compute the J-integral. To account for the stress singularity at the crack tip under the framework of LEFM, the mid-side

node parameter is set to 0.25, and the degenerate element side with a single node is selected. The accuracy of the calculated J-integral values and the local stress and strain fields is enhanced when singularity is incorporated into the meshes at the crack tip in small-strain analysis, compared to cases where no singularity is included. As stated before, the $1/\sqrt{r}$ singularity occurs in LEFM, which requires shifting the nodes to quarter position, achieved by setting the mid-side node parameter to 0.25. Once the plate geometry, polygonal void, and crack are defined, the script applies boundary conditions and initiates the meshing process. A localized seeding strategy is employed to ensure a denser mesh near the crack tip, as depicted in **Figure 4**, effectively capturing stress intensity factors while avoiding an excessive increase in the total element count for the model. Utilizing spider-web meshing around the crack tip enables the use of any reasonable number of contours to accurately compute the J-integral and the stress intensity factors. For this purpose, the meshing technique within the circular region around the crack tip is designated as "sweep," while the remaining parts of the geometry are meshed using the "free" meshing technique. After each simulation run, the values corresponding to the first two fracture modes are extracted and stored in a .CSV file alongside the four input parameters: the polygon's number of vertices, angle, average radius, and crack length.

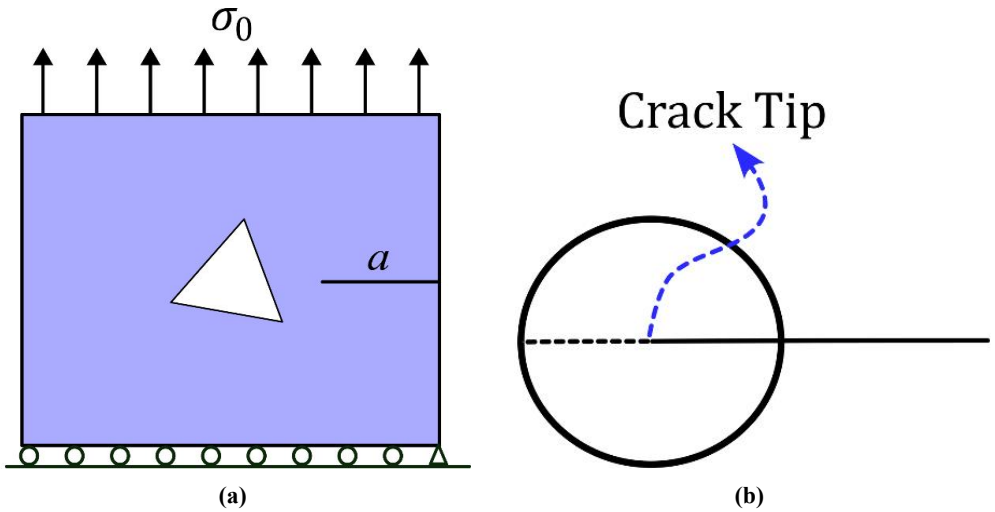

Figure 3. **(a)** Geometry, loading, and boundary condition of a single-edge cracked plate with polygon-shaped void; **(b)** Partitioning around the crack tip.

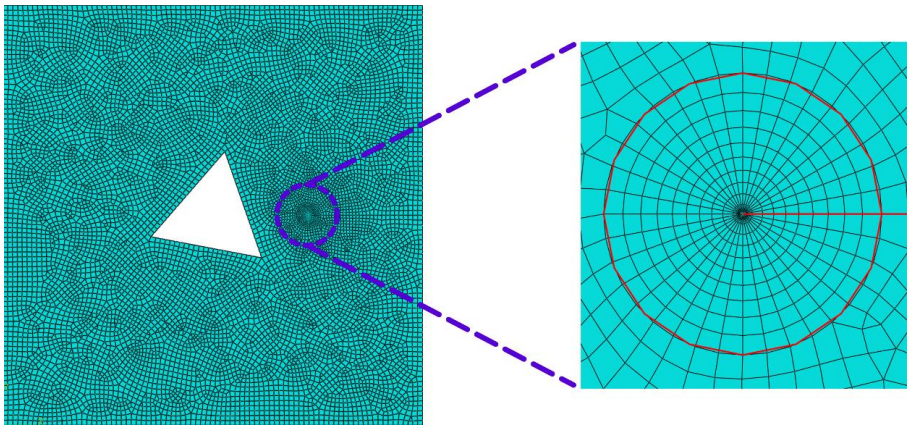

Figure 4. Meshing of a single-edge cracked plate with a polygon-shaped void.

3. Machine learning algorithms

In this section, the mathematical formulations and methodologies of the employed machine learning algorithms are detailed. Two distinct approaches are explored: the group method of data handling network, discussed in Section 3.1, and the artificial neural network, explained in Section 3.2.

3.1. GMDH

The group method of data handling, introduced by Ivakhnenko [35,36], provides a robust framework for modeling complex systems through multivariate analysis. It employs the Kolmogorov-Gabor polynomial to approximate the relationship between input and output variables. By employing a perceptron-inspired iterative structure, GMDH reconstructs polynomial models, thereby optimizing computational efficiency and improving accuracy. Although higher-order polynomials can be utilized to enhance system complexity, the quadratic polynomial with six weighting coefficients is often deemed sufficient for many engineering applications due to its simplicity and reliability [37]. GMDH incorporates mathematical modeling, nonlinear regression, and natural selection principles to regulate the network's size, complexity, and precision. The GMDH methodology simplifies complex problems through a divide-and-conquer strategy by decomposing them into smaller patterns and reassembling them through algebraic operations like sorting, addition, multiplication, crossing, and selection, where crossing and selection techniques are similarly utilized in meta-heuristic algorithms like Genetic Algorithm (GA) or Particle Swarm Optimization (PSO) [38]. The network architecture of GMDH evolves adaptively during training and comprises input, hidden, and output layers. Neurons within these layers are connected by quadratic polynomials, generating new neurons in subsequent layers to iteratively refine the model. Each node's activation function is derived from elementary polynomials, and the training process minimizes the least squares error between predicted and actual outputs. By employing an approximate function $\widehat{f}$, GMDH enables accurate predictions of outputs $\widehat{y}$ for given input vector $\mathbf{X} = (x_1, x_2, \ldots, x_N)$ as [37,39,40],

$$\widehat{y} = \widehat{f}\left(x_{i1}, x_{i2} \ldots, x_{iN}\right), \quad i = 1,\ 2,\ \ldots,\ M \tag{8}$$

where M is the number of data samples, and N is the number of input variables. Additionally, this Kolmogorov-Gabor type polynomial has the form,

$$\widehat{y} = a_0 + \sum_{i=1}^{N} a_i x_i + \sum_{i=1}^{N}\sum_{j=1}^{N} a_{ij} x_i x_j + \sum_{i=1}^{N}\sum_{j=1}^{N}\sum_{k=1}^{N} a_{ijk} x_i x_j x_k + \ldots \tag{9}$$

in which a represents the constant coefficients of this model. The objective is to construct a GMDH-type neural network such that the root mean squared error (RMSE) between the actual output and the predicted output is minimized. Mathematically, this optimization problem can be expressed as,

$$\text{RMSE} = \sqrt{\frac{\sum_{i=1}^{M}\left[\widehat{f}\left(x_{i1}, x_{i2}\ldots, x_{iN}\right) - y_i\right]^2}{M}} \rightarrow \text{min} \tag{10}$$

Employing the divide-and-conquer strategy, in this network, each neuron is designed to process only two input variables, producing an output by combining these inputs through a specific mathematical operation. The second-order Ivakhnenko polynomial used for each neuron as a sub-expression is [39],

$$z_{ij} = c_0 + c_1 x_i + c_2 x_j + c_3 x_i^2 + c_4 x_j^2 + c_5 x_i x_j \tag{11}$$

where z is the output of each neuron. The coefficients c_0 to c_5 of this submodel are determined using the least squares method. Since the network produces a single output, which aims to predict the true value y, the objective is to minimize the error between the true output y and the output of each neuron z in any given neuron. This is achieved by adjusting c_0 to c_5 through the least squares method as detailed below. For a single neuron with input variables x_i and x_j and considering one sample, this problem is stated as,

$$y \approx z = [c_0\ c_1\ c_2\ c_3\ c_4\ c_5] \begin{bmatrix} 1 \\ x_i \\ x_j \\ x_i^2 \\ x_j^2 \\ x_i x_j \end{bmatrix} \rightarrow y_{1\times 1} = c_{1\times 6}^{T} \mathrm{X}_{6\times 1} \tag{12}$$

Since this neuron should apply to all data samples, Equation (12) can be extended as,

$$\left.\begin{array}{l} y_1 = c^{\mathrm{T}} \mathrm{X}_1 \\ y_2 = c^{\mathrm{T}} \mathrm{X}_2 \\ \vdots \\ y_m = c^{\mathrm{T}} \mathrm{X}_m \end{array}\right\} \rightarrow [y_1\ y_2 \ldots y_m]_{1\times m} = C_{1\times 6}^{\mathrm{T}} [\mathrm{X}_1\ \mathrm{X}_2 \ldots \mathrm{X}_{\mathrm{m}}]_{6\times m} \rightarrow \mathbf{Y} = \mathbf{C}^{\mathrm{T}}\mathbf{X} \tag{13}$$

here, $\mathbf{X}$ represents the regressors matrix. To solve for the coefficient vector $\mathbf{C}$, it is necessary to ensure that the number of samples m is greater than or equal to the number of unknowns. This condition ($m \geq 6$) guarantees that the system of equations is either determined or overdetermined, and consequently $\mathbf{X}\mathbf{X}^{\mathrm{T}}$ becomes a full-rank matrix and has an inverse. Considering this, one can write,

$$\mathbf{Y} = \mathbf{C}^{\mathrm{T}}\mathbf{X} \rightarrow \mathbf{Y}\mathbf{X}^{\mathrm{T}} = \mathbf{C}^{\mathrm{T}}\mathbf{X}\mathbf{X}^{\mathrm{T}} \xrightarrow{\times(\mathbf{X}\mathbf{X}^{\mathrm{T}})^{-1}} \mathbf{Y}\mathbf{X}^{\mathrm{T}}(\mathbf{X}\mathbf{X}^{\mathrm{T}})^{-1} = \mathbf{C}^{\mathrm{T}}\mathbf{X}\mathbf{X}^{\mathrm{T}}(\mathbf{X}\mathbf{X}^{\mathrm{T}})^{-1} \rightarrow \mathbf{C}^{\mathrm{T}} = \mathbf{Y}\mathbf{X}^{\mathrm{T}}(\mathbf{X}\mathbf{X}^{\mathrm{T}})^{-1} \tag{14}$$

where $\mathbf{X}^{\mathrm{T}}\left(\mathbf{X}\mathbf{X}^{\mathrm{T}}\right)^{-1}$ is the right psedu-inverse, and is denoted by $\mathbf{X}^{\dagger}$. Finally, the coefficients vector can be expressed as

$$\mathbf{C}^{\mathrm{T}} = \mathbf{Y}\mathbf{X}^{\dagger} \tag{15}$$

The input data are normalized and scaled to the [1] range before being fed into the network to calculate the coefficient vector **C**. This normalization is performed using the following equation

$$X_{norm} = \frac{X - X_{min}}{X_{max} - X_{min}} \tag{16}$$

Here, X_{min} and X_{max} represent the minimum and maximum values of the input variable X, respectively. Normalization ensures that all input features contribute equally during training and improves the numerical stability and convergence rate of the network.

Prior to the training process of the GMDH network, the dataset is partitioned into three subsets: training, testing, and validation data. The training data is employed to calculate the coefficients c_0 to c_5 for each neuron utilizing the least squares method, optimizing the network's internal parameters. Simultaneously, the test data is used to evaluate the performance of the neurons based on the RMSE criterion, allowing the network to retain the best-performing neurons while discarding less effective ones. In this work, 70% of all data is allocated for training purposes (training and test datasets). Finally, the validation data, which remains unseen during training and testing, is used exclusively to assess the network's performance, ensuring the model's generalization capability and preventing overfitting. A total of 30% of the data is designated as the validation dataset. The remaining 70% of the data, utilized for training purposes, is further split into two subsets: 70% of this portion is allocated for training, and the remaining 30% is assigned as the test dataset.

3.2. ANN

The goal of this model is to develop an artificial neural network model capable of predicting the stress intensity factors K_I and K_{II} in the problem in hand. The dataset used contains key features such as the number of edges, angle of void on the plate, average radius, and crack length, mapped to corresponding K_I and K_{II} values. The dataset is first preprocessed and split into training and test sets to ensure robust evaluation. Data standardization is applied to normalize feature scales, improving the model's convergence during training. Standardization is performed on both the input features and target variables to ensure uniform scaling and improve the model's convergence during training. This step is necessary because features with varying scales can disproportionately influence the optimization process, leading to slower convergence or suboptimal results. To train the ANN network, dataset is normalized utilizing Equation (17) as,

$$z = \frac{x - \mu}{\sigma_{std}} \tag{17}$$

where z is the standardized value, x is the original value, is the mean of the feature, and σ_{std} is the standard deviation of the feature. The dataset is then split into training

(80%) and testing (20%) subsets using scikit-learn, with a fixed random state to ensure reproducibility. This split allowed the model to learn from the training data and validate its performance on unseen testing data.

The ANN employed for predicting K_I and K_{II} is designed to capture the underlying relationships between the input features and the target variables. The architecture has an input layer consisting of four features. Two hidden layers are included to capture complex, non-linear relationships in the data. These layers are equipped with ReLU (Rectified Linear Unit) activation functions to introduce non-linearity and avoid issues like vanishing gradients during training. 32 neurons are chosen for the first hidden layer, and 16 neurons are subsequently used in the second hidden layer to progressively refine the learned representations. The output layer consists of 2 neurons, each corresponding to one of the target variables K_I and K_{II}. The two hidden layers strike a balance between model complexity and overfitting prevention, providing sufficient depth for learning complex relationships without over-parameterization. Additionally, the number of neurons in each layer is selected based on experimentation to achieve optimal model performance while avoiding overfitting or underfitting. As the final step, the neural network model is trained using the Adam optimizer, a widely used optimization algorithm that adapts learning rates for each parameter to improve convergence.

4. Results and discussion

In this section, the machine learning algorithms are applied on the dataset generated through Abaqus simulations, as detailed in the previous sections. The goal is to predict the mode I and mode II stress intensity factors of fracture using the four input parameters: polygon's number of vertices, angle, average radius, and crack length. The results are analyzed to evaluate the performance and accuracy of the models in capturing the underlying relationships within the data. The subsequent structure for the machine learning solutions is utilized,

$$\begin{cases} \text{Input variables: } \mathbf{x} = (x_1, x_2, x_3, x_4) = (\text{num verts, angle, avg radius, crack length}) \\ \text{Target variables: } \mathbf{y} = (y_1, y_2) = (K_I, K_{II}) \end{cases}$$

To emphasize the impact of the central polygon-shaped void on the calculation of stress intensity factors, **Tables 2** and **3** present the K_I and K_{II} values, sequentially, for scenarios with and without the inclusion of polygons. These tables also explore variations in the number of vertices and crack lengths, providing a comprehensive assessment of how the presence of polygonal voids influence the fracture behavior of the plate. In this scrutiny, polygon-shaped voids are considered with an angle of 0 rad and an average radius of 40 mm. It is seen that the existence of a central void has an intensifying effect on the K_I values, while K_{II} values are reduced by considering the void, indicating the protective effect of introducing a void to the left side of the crack and mitigating the possibility of fracture under in-plane shear loading.

Table 2. The intensification effect of central polygon-shaped voids on the K_I values $(MPa\sqrt{mm})$.

Crack length (mm)	50	55	60	65	70
$\boldsymbol{K_I}$ without polygon	1763.15	1918.25	2080.96	2252.17	2434.14
$\boldsymbol{K_I}$ 3 vertices	1947.88	2175.88	2429.00	2729.18	3100.63
$\boldsymbol{K_I}$ 5 vertices	2008.88	2270.09	2567.25	2926.68	3381.12
$\boldsymbol{K_I}$ 7 vertices	2074.14	2356.95	2684.30	3085.80	3599.25
$\boldsymbol{K_I}$ 9 vertices	2104.83	2399.72	2748.03	3174.85	3736.90

Table 3. Protective effect of central polygon-shaped voids on the K_{II} values $(MPa\sqrt{mm})$.

Crack length (mm)	50	55	60	65	70
$\boldsymbol{K_{II}}$ without polygon	45.79	59.47	75.94	94.08	112.88
$\boldsymbol{K_{II}}$ 3 vertices	12.74	26.09	44.18	67.00	96.40
$\boldsymbol{K_{II}}$ 5 vertices	−2.75	12.16	32.44	59.04	96.28
$\boldsymbol{K_{II}}$ 7 vertices	−9.65	6.07	28.13	57.53	99.67
$\boldsymbol{K_{II}}$ 9 vertices	−11.49	4.52	26.97	54.89	98.48

It should be noted that K_{II} may take positive or negative values depending on the direction of the local shear traction at the crack tip. In the present study, the sign of K_{II} was found to change for certain polygon configurations due to the strong asymmetry of the stress field induced by the void geometry. The interaction-integral formulation in Abaqus was employed with consistent crack-tip orientation, and both the magnitude and sign of K_I and K_{II} were verified to be independent of contour number and mesh refinement.

To introduce a comprehensive machine learning framework for prediction of stress intensity factors for opening and in-plane shear fracture modes, first, a simple GMDH network with the structure of $(4, 2, 1)$ is considered, indicating that four input variables feed into the first and only hidden layer, producing the two best-performing neurons. These neurons are then integrated into the final layer to produce the output. Separate GMDH networks are trained for K_I and K_{II} values as outputs, both employing the aforementioned structure. For the K_I network, the correlation coefficient is $R = 0.983$, and the RMSE on the validation dataset is 69.6. The GMDH algorithm automatically selects the optimal neurons in each layer based on the lowest RMSE, discarding less effective neurons. In this case, the two selected neurons in the first hidden layer correspond to the pairs (average radius, crack length) and (number of vertices, crack length). This indicates that the polygon's angle has a negligible effect on K_I, while the crack length significantly influences it. This simple GMDH network demonstrates reasonable accuracy in predicting the mode I stress intensity factor. For K_{II}, the same GMDH network structure is applied, yielding a correlation coefficient of $R = 0.694$ and an RMSE of 39.1. For this network, the two selected neurons in the first hidden layer correspond to the pairs (angle, crack length) and (number of vertices, angle), showcasing the importance of angle of central polygon in predicting the mode II SIFs. These results suggest that this simple GMDH network does not provide sufficiently accurate predictions for K_{II}. **Figure 5** further illustrates the predictions of this GMDH network structure with one hidden layer for various validation data points.

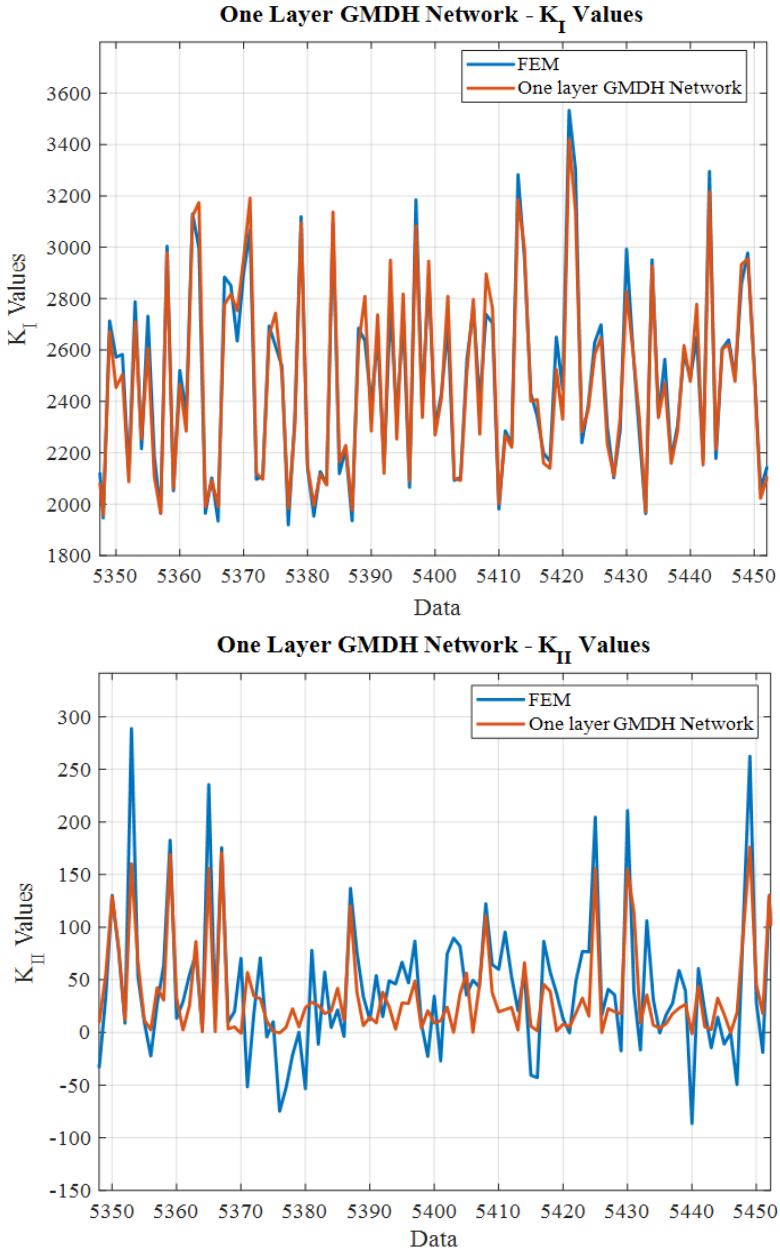

Figure 5. Performance of GMDH network consisting of one hidden layer.

A more complex GMDH network with a structure of $(4,\ 6,\ 15,\ 50,\ 50,\ 50,\ 50,\ 50,\ 50,\ 50,\ 50,\ 1)$ is considered, representing the number of neurons in each layer sequentially. To manage the network's size and complexity, a constraint is applied at each layer, retaining only the best fifty neurons based on RMSE performance. Two separate networks are trained to predict the mode I (K_I) and mode II (K_{II}) stress intensity factors. For K_I, the network achieves a high correlation factor of $R = 0.998$ and an RMSE of 20.61, demonstrating satisfactory predictive accuracy. Similarly, the network for K_{II} displays a notable improvement, achieving a correlation factor of $R = 0.86$ and an RMSE of 27.68. The performance of these networks is illustrated in **Figure 6**, which highlights the enhanced accuracy of this GMDH structure compared to the simpler network, particularly in predicting K_{II}. However, the increased accuracy comes at the cost of higher computational complexity due to the more intricate polynomial functions generated by this deeper network. To assess the influence of

individual input parameters on the performance of the GMDH network, the model was trained using three input parameters for predicting K_I and K_{II} values. For K_I, excluding the number of vertices resulted in a moderate impact, while excluding the average radius significantly affected the outcomes, highlighting its critical role in the predictions. The most influential parameter for K_I was the crack length where its omission led to a drastic reduction in prediction accuracy. For K_{II}, the exclusion of any single parameter caused a noticeable decline in performance, with the angle identified as the most influential input, reflecting its substantial effect on the prediction of mode II stress intensity factors. The relatively weak influence of polygon orientation on K_I, as compared to its pronounced effect on K_{II}, is inferred from the consistent behavior observed across the entire FEM dataset and the structure-selection process of the GMDH model. While a dedicated one-parameter sweep of the polygon angle at fixed geometry would provide further quantitative insight, such an ablation study is beyond the scope of the present work and is suggested for future investigation.

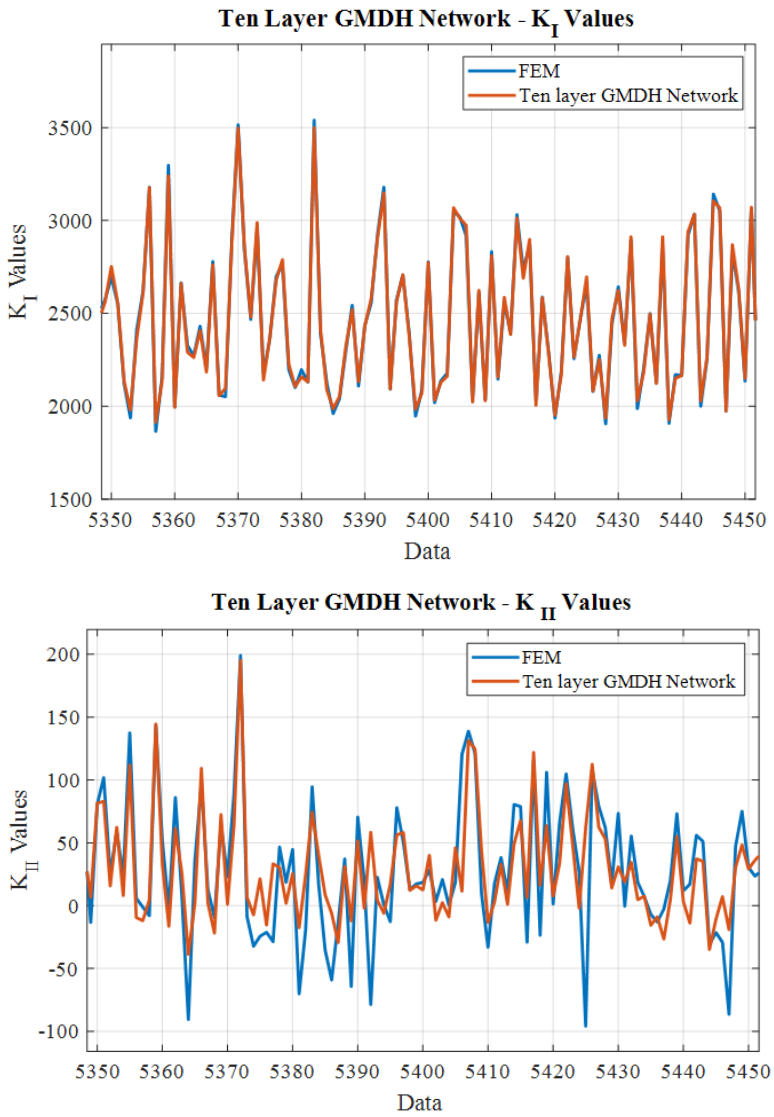

Figure 6. Performance of GMDH network consisting of ten hidden layers.

After training and analyzing the GMDH networks, a feed forward fully connected ANN is trained and evaluated. The training process spanned 50 epochs with a batch

size of 32, ensuring efficient gradient updates. To monitor the model's performance and mitigate overfitting, 20% of the training set is allocated as validation data. During each epoch, the model's Mean Squared Error (MSE) and Mean Absolute Error (MAE) metrics are computed to assess its accuracy and loss. The implementation utilized TensorFlow and Keras, powerful deep learning libraries, to define, train, and evaluate the model seamlessly. These libraries facilitate efficient computation and easy integration of scaling, splitting, and visualization tasks. The training and validation losses are indicated in **Figure 7**. For this network, the model's performance is assessed on the test dataset, indicating MSE as 216.69 for K_I and 40.27 for K_{II}. The MAE for K_I and K_{II} values are 11.10 and 4.71, respectively. The R-squared (R^2) criterion of this model for mode I and II SIF predictions are also 0.9985 and 0.9868, sequentially. These values indicate excellent performance of ANN in predicting stress intensity factors of mode I and II fractures.

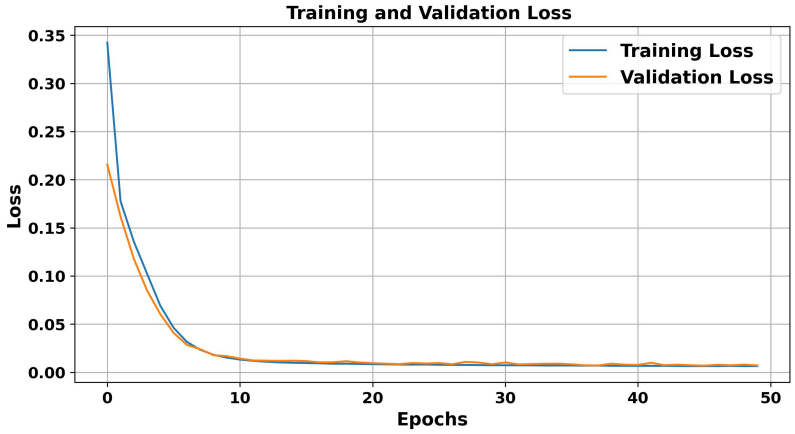

Figure 7. Loss values for the ANN training process.

Figure 8 illustrates the regression distribution of predicted versus true values for K_I and K_{II} using three models: GMDH with one hidden layer, GMDH with ten hidden layers, and the ANN network. The ideal prediction corresponds to the $y = x$ line. For K_I, the ANN network demonstrates the highest performance, achieving $R^2 = 0.998$ and $MAE = 11.1$, followed closely by the ten-layer GMDH network with $R^2 = 0.997$ and $MAE = 15.5$. The one-layer GMDH model, while delivering acceptable results, lags significantly with $R^2 = 0.968$ and $MAE = 51.58$. For K_{II}, ANN again outperforms the GMDH models with $R^2 = 0.986$ and $MAE = 4.71$. The ten-layer GMDH network exhibits moderate performance with $R^2 = 0.746$ and $MAE = 19.7$, whereas the one-layer GMDH network struggles to accurately predict K_{II}, showing $R^2 = 0.481$ and $MAE = 29.63$. This shows the inability of the GMDH polynomial network to effectively capture the nonlinear relationships governing K_{II}, while ANN demonstrates superior accuracy for both fracture modes. Comparison of true and predicted K_I and K_{II} values is provided in **Figure 9**. It is seen that ANN is capable of estimating SIF values with excellent accuracy.

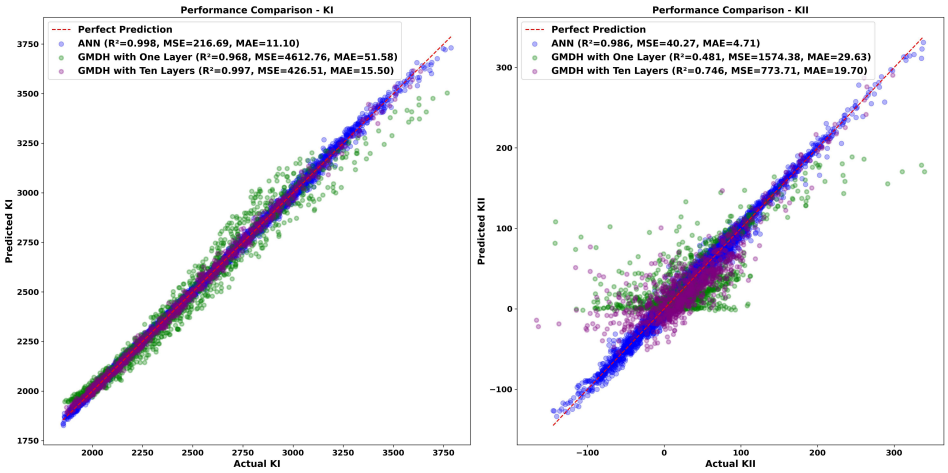

Figure 8. The correlation diagram comparing actual and predicted values of K_I and K_{II}.

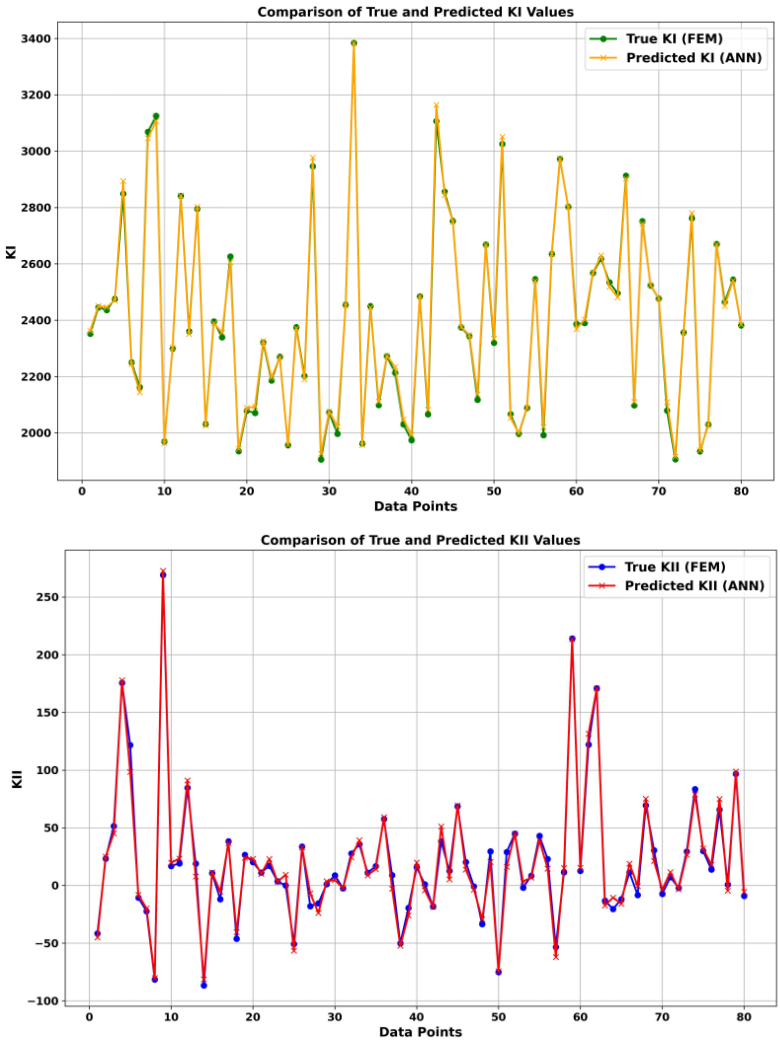

Figure 9. Performance of ANN in predicting mode I and II stress intensity factors.

One key feature of any regression-based machine learning algorithm is its capability to perform interpolation and extrapolation predictions on the newly generated data. To this aim, a numerical scrutiny is conducted on a new mini-dataset consisting of five data points. Stress intensity factors for mode I and II of fracture are estimated in **Figure 10**. Comparing the true values with the GMDH and ANN predictions, it is seen

that ANN has the capability to predict both fracture modes SIF, while GMDH fails to predict K_{II} values and exhibits lower accuracy in interpolation and extrapolation predictions comparing to the ANN.

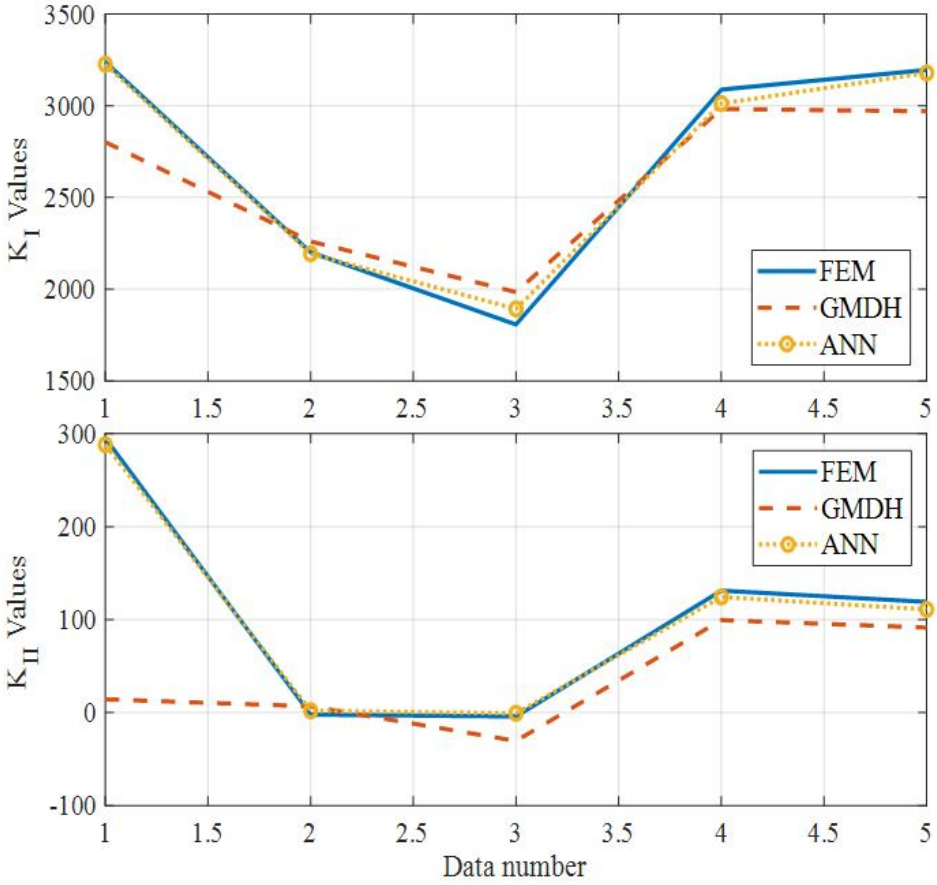

Figure 10. Comparison between interpolation and extrapolation performance of GMDH and ANN.

5. Conclusion

This study presents a comprehensive framework for predicting the mode I and mode II stress intensity factors of a single-edge cracked plate with polygon-shaped voids, utilizing machine learning algorithms and finite element analysis. A dataset was generated using Abaqus simulations, capturing the effects of four critical input parameters: the polygon's number of vertices, angle, average radius, and crack length. A GMDH network was initially employed, demonstrating reasonable accuracy in predicting K_I but struggling to capture the nonlinear relationships governing K_{II}. The performance improved significantly with a deeper GMDH network, achieving higher accuracy, particularly for K_{II} predictions, albeit at the cost of increased computational complexity. The influence of individual input parameters was also evaluated, highlighting crack length as the most critical parameter for K_I predictions and the polygon's angle as the most significant for K_{II}. Subsequently, a feed-forward fully connected artificial neural network was trained and evaluated. The ANN outperformed the GMDH networks in both fracture modes, achieving superior R^2 values and lower error metrics. The regression analysis confirmed the ANN's ability

to accurately capture the nonlinear relationships between input features and SIFs, as evidenced by its exceptional performance on validation datasets. The ANN also demonstrated robust interpolation and extrapolation capabilities, predicting SIF values with remarkable accuracy for new data points, while the GMDH models exhibited limitations, particularly for K_{II}.

Author contributions: MZE: Methodology, Software, Validation, Visualization, Writing—original draft. SN: Data curation, Project administration, Resources, Supervision, Writing—review and editing. MAS: Resources, Supervision, Writing—review and editing. AA: Formal analysis, Investigation, Visualization, Writing—original draft. RA: Conceptualization, Formal analysis, Project administration, Supervision, Writing—original draft. All authors have read and agreed to the published version of the manuscript.

Funding: The authors received no financial support for the research, authorship, and publication of this article.

Institutional review board statement: Not applicable.

Informed consent statement: Not applicable.

Data availability statement: The data that support the findings of this study are available on request from the corresponding author. The data are not publicly available due to privacy or ethical restrictions.

Conflict of interest: The authors declare no conflict of interest.

References

1. Sumpter JDG, Kent JS. Prediction of ship brittle fracture casualty rates by a probabilistic method. Marine Structures. 2004; 17(8): 575–589. doi: 10.1016/J.MARSTRUC.2005.03.003
2. Inglis CE. Stresses in a plate due to the presence of cracks and sharp corners. Transactions of the Institution of Naval Architects. 1913; 55: 219–241.
3. Griffith AA. The phenomena of rupture and flow in solids. Philosophical Transactions of the Royal Society of London Series A, Containing Papers of a Mathematical or Physical Character. 1921; 221: 163–198.
4. Ibrahim RA. Overview of structural life assessment and reliability, part I: Basic ingredients of fracture mechanics. Journal of Ship Production and Design. 2015; 31(1): 1–42. doi: 10.5957/JSPD.2015.31.1.1
5. Ferrian F, Cornetti P, Sapora A, et al. Crack tip shielding and size effect related to parallel edge cracks under uniaxial tensile loading. International Journal of Fracture. 2024; 245(3): 223–233. doi: 10.1007/S10704-023-00756-1
6. Rice JR. A path independent integral and the approximate analysis of strain concentration by notches and cracks. Journal of Applied Mechanics. 1968; 35(2): 379–386. doi: 10.1115/1.3601206
7. Li Y, Ni T, Zhang F, et al. U-Net learning for the automatic identification of the sandstone crack tip position to determine mixed-mode stress intensity factors utilizing digital image correlation method. Theoretical and Applied Fracture Mechanics. 2023; 127: 104028. doi: 10.1016/J.TAFMEC.2023.104028
8. Xiao H, Xie Y, Yue Z. Analysis of square-shaped crack in layered halfspace subject to uniform loading over rectangular surface area. Computer Modeling in Engineering and Sciences. 2015; 109–110(1): 55–80. doi: 10.3970/CMES.2015.109.055
9. Kumar SS, Prakash RV. Stress intensity factor solution for a naturally emanating crack out of a V-notched round bar. International Journal for Computational Methods in Engineering Science and Mechanics. 2015; 16(5): 301–312. doi: 10.1080/15502287.2015.1080319
10. Fardaghaie A, Shahrooi S, Shishehsaz M. A novel correlation to calculate stress intensity factors of the semi-elliptical

crack in high-strength carbon steel pipe based on extended isogeometric analysis. Journal of the Brazilian Society of Mechanical Sciences and Engineering. 2022; 44(1): 50. doi: 10.1007/S40430-021-03343-4
11. Tang SB. Stress intensity factors for a Brazilian disc with a central crack subjected to compression. International Journal of Rock Mechanics and Mining Sciences. 2017; 93: 38–45. doi: 10.1016/J.IJRMMS.2017.01.003
12. Dong S. Theoretical analysis of the effects of relative crack length and loading angle on the experimental results for cracked Brazilian disk testing. Engineering Fracture Mechanics. 2008; 75(8): 2575–2581. doi: 10.1016/J.ENGFRACMECH.2007.09.008
13. Hassani Niaki M, Pashaian M. Using deep learning method to predict dimensionless values of stress intensity factors and *T*-stress of edge notch disk bend specimen. Fatigue and Fracture of Engineering Materials and Structures. 2024; 47(8): 2789–2802. doi: 10.1111/FFE.14330
14. Bert CW, Malik M. Differential quadrature: a powerful new technique for analysis of composite structures. Composite Structures. 1997; 39(3–4): 179–189.
15. Kabir H, Aghdam MM. A generalized 2D Bézier-based solution for stress analysis of notched epoxy resin plates reinforced with graphene nanoplatelets. Thin-Walled Structures. 2021; 169: 108484.
16. Coelho JS, Machado MR, Dutkiewicz M, et al. Data-driven machine learning for pattern recognition and detection of loosening torque in bolted joints. Journal of the Brazilian Society of Mechanical Sciences and Engineering. 2024; 46(2): 75. doi: 10.1007/S40430-023-04628-6
17. Zheng M, Yu J. Parametric optimization and determination in machining processes by means of probabilistic multi-objective optimization. Mechanical Engineering Advances. 2025; 3(1). doi: 10.59400/MEA1950
18. Moore BA, Rougier E, O'Malley D, et al. Predictive modeling of dynamic fracture growth in brittle materials with machine learning. Computational Materials Science. 2018; 148: 46–53. doi: 10.1016/J.COMMATSCI.2018.01.056
19. Jiang S, Du J, Wang S, et al. Risk assessment of initial crack propagation in bearing steel based on finite element analysis and machine learning. Mechanics Based Design of Structures and Machines. 2024; 53(5): 3619–3634. doi: 10.1080/15397734.2024.2429738
20. Kim KB, Yoon DJ, Jeong JC, et al. Determining the stress intensity factor of a material with an artificial neural network from acoustic emission measurements. NDT and E International. 2004; 37(6): 423–429. doi: 10.1016/J.NDTEINT.2003.08.007
21. Liu X, Athanasiou CE, Padture NP, et al. A machine learning approach to fracture mechanics problems. Acta Materialia. 2020; 190: 105–112. doi: 10.1016/J.ACTAMAT.2020.03.016
22. Talebi H, Bahrami B, Daneshfar M, et al. Data-driven based fracture prediction of notched components. Philosophical Transactions of the Royal Society A. 2024; 382(2264): 20220397. doi: 10.1098/RSTA.2022.0397
23. Kaloop MR, Samui P, Kim JJ, et al. Stress intensity factor prediction on offshore pipelines using surrogate modeling techniques. Case Studies in Construction Materials. 2022; 16: e01045. doi: 10.1016/J.CSCM.2022.E01045
24. Zhang X, Zhao T, Liu Y, et al. A data-driven model for predicting the mixed-mode stress intensity factors of a crack in composites. Engineering Fracture Mechanics. 2023; 288: 109385. doi: 10.1016/J.ENGFRACMECH.2023.109385
25. Parsania A, Kakavand E, Hosseini SA, et al. Estimation of multiple cracks interaction and its effect on stress intensity factors under mixed load by artificial neural networks. Theoretical and Applied Fracture Mechanics. 2024; 131: 104340. doi: 10.1016/J.TAFMEC.2024.104340
26. Williams ML. On the stress distribution at the base of a stationary crack. Journal of Applied Mechanics. 1957; 24(1): 109–114. doi: 10.1115/1.4011454
27. Irwin GR. Analysis of stresses and strains near the end of a crack traversing a plate. Journal of Applied Mechanics. 1957; 24(3): 361–364. doi: 10.1115/1.4011547
28. Tada H, Paris PC, Irwin GR. The Stress Analysis of Cracks Handbook, 3rd ed. ASME Press; 2000. doi: 10.1115/1.801535
29. ASTM International Committee E08 on Fatigue and Fracture. Standard Test Method for Linear-elastic Plane-strain Fracture Toughness KIC of Metallic Materials. ASTM International; 2013.
30. Algorithm to generate random 2D polygon. Available online: https://stackoverflow.com/questions/8997099/algorithm-to-generate-random-2d-polygon (accessed on 10 December 2024).
31. Rezasefat M, Hogan JD. A finite element-convolutional neural network model (FE-CNN) for stress field analysis around arbitrary inclusions. Machine Learning: Science and Technology. 2023; 4(4): 045052. doi: 10.1088/2632-2153/AD134A
32. Alshoaibi AM, Ariffin AK. Finite element simulation of stress intensity factors in elastic-plastic crack growth. Journal of Zhejiang University SCIENCE A. 2006; 7(8): 1336–1342. doi: 10.1631/JZUS.2006.A1336

33. Rao BN, Rahman S. A coupled meshless-finite element method for fracture analysis of cracks. International Journal of Pressure Vessels and Piping. 2001; 78(9): 647–657. doi: 10.1016/S0308-0161(01)00076-X
34. Yan X. An empirical formula for stress intensity factors of cracks emanating from a circular hole in a rectangular plate in tension. Engineering Failure Analysis. 2007; 14(5): 935–940. doi: 10.1016/J.ENGFAILANAL.2006.11.008
35. Ivakhnenko AG. Heuristic self-organization in problems of engineering cybernetics. Automatica. 1970; 6(2): 207–219. doi: 10.1016/0005-1098(70)90092-0
36. Ivakhnenko AG. Polynomial theory of complex systems. IEEE Transactions on Systems, Man, and Cybernetics. 1971; 1(4): 364–378. doi: 10.1109/TSMC.1971.4308320
37. Madandoust R, Bungey JH, Ghavidel R. Prediction of the concrete compressive strength by means of core testing using GMDH-type neural network and ANFIS models. Computational Materials Science. 2012; 51(1): 261–272. doi: 10.1016/J.COMMATSCI.2011.07.053
38. Panoiu M, Panoiu C, Rusu-Anghel S, et al. Modeling the pantograph-catenary contact in electric railway transportation using group method of data handling. In: Proceedings of the IECON Industrial Electronics Conference; 14–17 October 2019; Lisbon, Portugal. doi: 10.1109/IECON.2019.8927244
39. Mostapha Kalami Heris. Group Method of Data Handling (GMDH) in MATLAB. Available online: https://yarpiz.com/263/ypml113-gmdh (accessed on 5 May 2025).
40. Hosseinian SM, Bazoobandi P, Mousavi SR, et al. Presentation of machine learning methods and multi-objective optimization of fracture indices for asphalt rubber mixtures containing wax-based warm mix additives modified by nano calcium carbonate. Construction and Building Materials. 2023; 409: 134136. doi: 10.1016/J.CONBUILDMAT.2023.134136